Bioorganic Chemistry 114 (2021) 105078

Contents lists available at ScienceDirect

Bioorganic Chemistry

journal homepage: www.elsevier.com/locate/bioorg

New pyrimidine and pyrazole-based compounds as potential EGFR inhibitors: Synthesis, anticancer, antimicrobial evaluation and computational studies

Ismail M.M. Othman [a], Zahra M. Alamshany [b], Nada Y. Tashkandi [b], Mohamed A. M. Gad-Elkareem [a], Manal M. Anwar [c,*], Eman S. Nossier [d]

[a] Department of Chemistry, Faculty of Science, Al-Azhar University, Assiut 71524, Egypt
[b] Department of Chemistry, Faculty of Science, King Abdulaziz University, Jeddah 21551, P.O. Box 42805, Saudi Arabia
[c] Department of Therapeutic Chemistry, National Research Centre, Dokki, Cairo 12622, Egypt
[d] Pharmaceutical Medicinal Chemistry and Drug Design Department, Faculty of Pharmacy (Girls), Al-Azhar University, Cairo 11754, Egypt

ARTICLE INFO

Keywords:
Pyrimidines
Pyrazoles
Cytotoxic
EGFR inhibition
Antibacterial
Antifungal
Molecular docking
ADMET prediction
MCF-7
HepG-2

ABSTRACT

This study was focused on the synthesis of new pyrimidines **4a,b, 5a,b** and pyrazoles **6a, b** as ATP mimicking tyrosine kinase inhibitors of the epidermal growth factor receptor (EGFR). The new compounds were assessed as cytotoxic candidates against human breast cancer cells (MCF-7) and hepatocellular carcinoma cells (HepG-2). All the new compounds appeared as more potent cytotoxic agents than erlotinib, while only compound **4a** exhibited more potency than 5-flourouracil and **4b** analogue was equipotent to it. Accordingly, the kinase suppression effect of **4a** and **4b** was further evaluated against $EGFR^{WT}$, $EGFR^{L858R}$ and $EGFR^{T790M}$. Both pyrimidine analogues **4a** and **4b** displayed outstanding inhibitory activity against $EGFR^{WT}$ and its two mutated isoforms $EGFR^{L858R}$ and $EGFR^{T790M}$ in comparing to erlotinib and osimertinib as reference drugs. Additionally, all the new analogues were subjected to antimicrobial assay. Interestingly, both **4a** and **4b** represented the most promising activity of wide spectrum antimicrobial effect against the examined microbes in comparison to gentamycin and ketoconazole as standard drugs. Moreover, docking results proved the good binding interactions of the compounds **4a** and **4b** with $EGFR^{WT}$ and $EGFR^{T790M}$ which were in accordance with the results of the *in vitro* enzyme assay. Additional *in silico* ADMET studies were performed for the new derivatives which represented their good oral absorption, good drug-likeness properties and low toxicity risks in human.

1. Introduction

Epidermal growth factor receptor (EGFR) is a receptor tyrosine kinase (RTK), belongs to ErbB family and performs a central role in signaling pathways of the cell such as; cell division, growth, differentiation, metabolism, adhesion, motility and death [1,2]. It is upregulated in multiple human malignancies, including non-small cell lung cancer (NSCLC), hepatocellular, colorectal, head and neck squamous cell carcinoma and breast cancers [3–5]. Different studies in the chemotherapeutic field showed that suppression of EGFR-TK introduces a rational basis for the development of a class of targeted therapies, EGFR-TK inhibitors (EGFR-TKIs). They act by competing with ATP for ATP-binding site on EGFR, thus blocking the signaling pathway leading to significant resistance to cancer cells, as well as angiogenesis, in addition to suppression of EGFR downstream PI3K/mTOR signaling pathway, leading to increase the lack of oxygen to improve the sensitivity of the cancer cells to radiation [6–8].

Despite the significant benefits of the first-generation EGFR inhibitors (**gefitinib** [9] and **erlotinib** [10]) in cancer treatment, the mutation in the ATP binding pocket of EGFR exon 20 leading to a threonine-to-methionine substitution at the amino acid position 790 (T790M) led to predominant drug resistance in 50% of cancer patients. At the same time, L858R mutation at exon 20 was detected as another mechanism of resistance to the first-generation EGFR-TKIs [8,11–13]. The second generation, irreversible TKIs including afatinib and dacomitinb containing a Michael acceptor functional group were developed to overcome these resistant tumor clones. However, due to low kinase selectivity between $EGFR^{T790M}$ mutation and $EGFR^{WT}$ (wild type EGFR),

* Corresponding author.
E-mail address: manal.hasan52@live.com (M.M. Anwar).

https://doi.org/10.1016/j.bioorg.2021.105078
Received 26 February 2021; Received in revised form 11 May 2021; Accepted 7 June 2021
Available online 10 June 2021

serious undesirable effects had occurred such as; skin rash and gastrointestinal toxicity which limited the clinical use of these inhibitors [14–17]. Accordingly, the third-generation EGFR inhibitors with pyrimidine core structures such as **WZ4002**, **rociletinib** and **osimertinib (AZD9291)** were created [18–21] (Fig. 1). Osimertinib is the only US FDA approved third-generation inhibitor, exhibiting a significant selectivity toward the drug-resistant mutant $EGFRT^{790M}$ over the wild-type EGFR ($EGFR^{WT}$), rendering it an important medical regimen for patients with $EGFR^{T790M}$ mutation [22]. Despite the excellent characteristics of osimertinib, it exhibited several adverse effects in clinical application, including diarrhea, rash, decreased appetite and cardiotoxicity [23–25]. Accordingly, there is still a great demand to develop new EGFR inhibitors with high selectivity against the $EGFR^{T790M}$ and $EGFR^{L858R}$ mutation to overcome the undesirable drawbacks and drug resistance.

The ATP binding active site of EGFR-TK is composed of five major regions (i) an adenine binding pocket which bears the key amino acids that create the H-bonding with the adenine ring, (ii) a sugar region which constitutes the hydrophilic pocket, (iii) hydrophobic region I, which is not exploited by ATP but plays a crucial role in inhibitor selectivity and binding affinity, (iv) hydrophobic region II which is not used by ATP and may be exploited for inhibitor specificity, and (v) a phosphate binding pocket which is largely solvent exposed and can be utilized for improving the pharmacokinetics of the inhibitor [26,27] (Fig. 2).

Different structure-activity relationship studies (SAR) represented that there are four common pharmacophoric features are shared by EGFR-TKIs: (i) a flat heterocyclic-aromatic ring system which interact with the adenine binding site and participates in H-bonding interactions with the corresponding amino acids, (ii) a terminal hydrophobic head for insertion in the hydrophobic pocket I, (iii) NH-linker that creates H-bonding with amino acid residues in the linker area, (iv) a hydrophobic tail which inserts into the hydrophobic area II [28–31] (Fig. 3).

Various literatures investigated that pyrimidine scaffold is an important building block in many antineoplastic agents via multi-suppression of different protein kinases including EGFR-TKs [4,32–34]. In addition, pyrazole and fused pyrazole systems were investigated as promising motifs in many antiproliferative agents against a broad range of cancers targeting the kinase inhibition activity of EGFR [35–37]. Various molecular simulation studies indicated that many pyrazole analogues fitted perfectly in the active pocket of EGFR kinase resulting in potent anticancer activity [38]. Accordingly, the

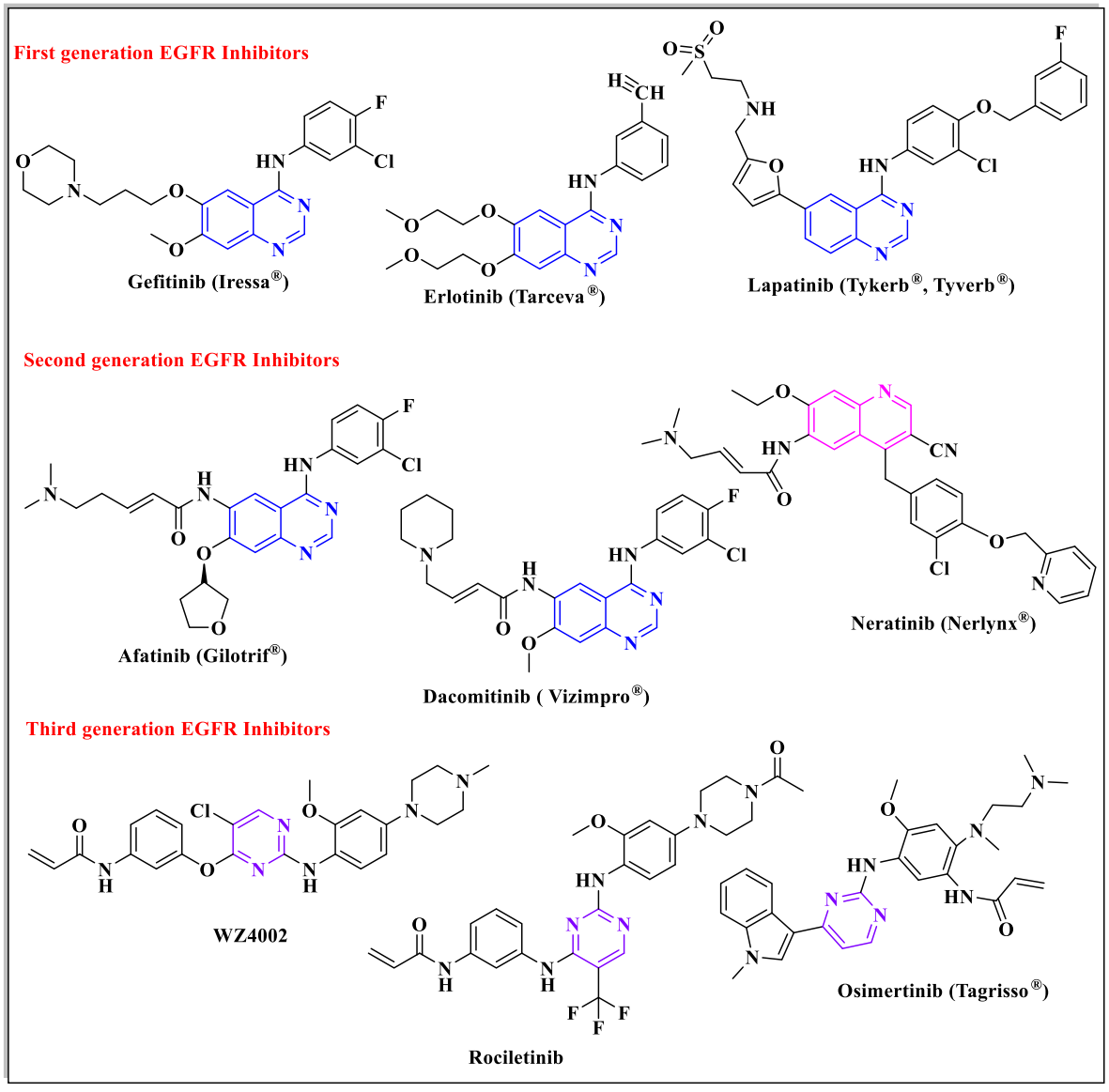

Fig. 1. The chemical structures of various drugs of EGFR tyrosine kinase inhibiting activity.

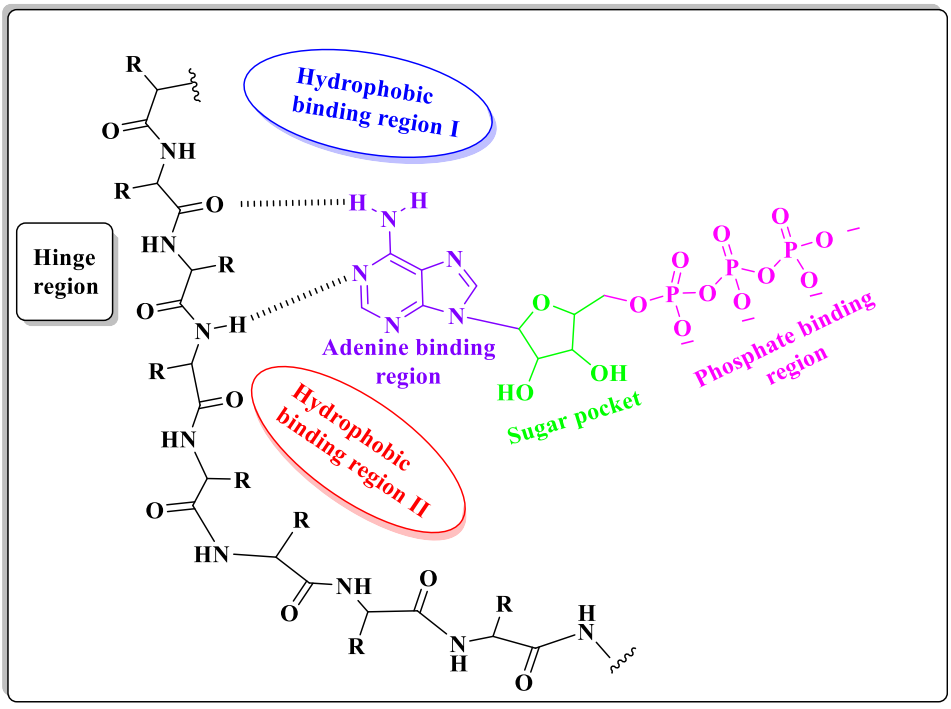

Fig. 2. The structure of ATP-binding site of EGFR-TK.

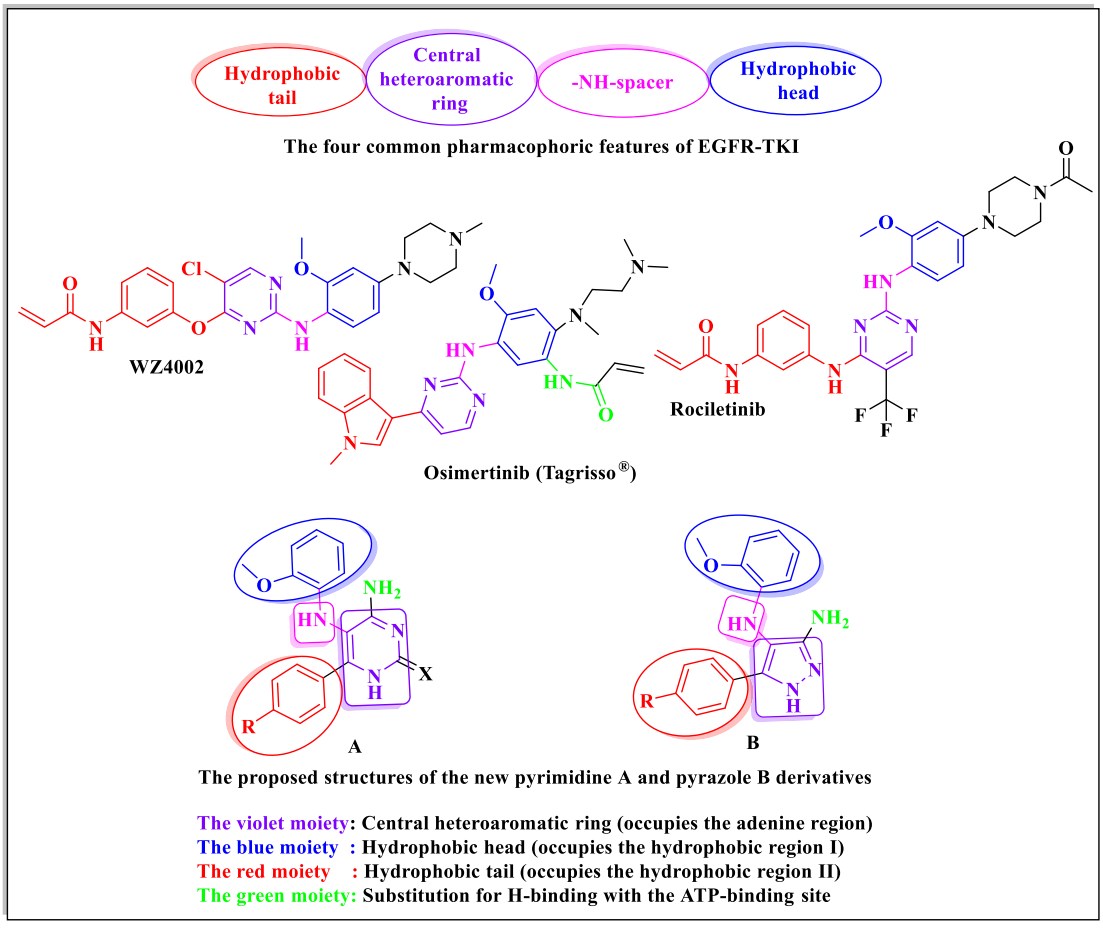

Fig. 3. Proposed hypothetic model of the new pyrimidine and pyrazole compounds as EGFR TKIs.

strategy of this work was focused on design and synthesis of new derivatives bearing pyrimidine-2-one(thione) or pyrazole motif having the essential pharmacophoric features of EGFR-TKIs. The first position was pyrimidine or pyrazole moieties (hetero-aromatic system) to occupy the adenine binding pocket. The second position was the terminal 2-methoxyphenyl ring (hydrophobic head). NH linker was utilized in the third position as a hydrogen bond donor. The fourth position was either phenyl or 4-tolyl rings incorporated at pyrimidine-C_6 or pyrazole-C_5 to occupy the hydrophobic region II of the ATP binding pocket (Fig. 3). its biological isostere pyrazole

All the newly synthesized compounds were evaluated as anticancer agents against human breast cancer cells (MCF-7) and human liver carcinoma cell line (HepG2). The compounds exhibited the most promising cytotoxic activity were evaluated for their ability to suppress the wild-type $EGFR^{WT}$ and the mutated isoforms $EGFR^{L858R}$ and $EGFRT^{790M}$. Furthermore, molecular docking study was performed for the promising derivatives to rationalize and emphasize their modes of action as EGFR-TKIs. In addition, *in silico* ADMET prediction was carried out for the new derivatives to explore their drug-likeness properties.

It is known that different types of cancers are essentially caused by various factors including certain types of infections [39]. Study of various antibiotic cytotoxic pharmaceutics including Actinomycin, Adriamycin/Doxorubicin and some other candidates revealed that in addition to DNA intercalating or DNA damaging effects, the stimulation of the existing host defense mechanism is considered as one of the approaches that these chemotherapeutics exert their antimicrobial effects [40]. Based on these evidences, in comparison to gentamycin and ketoconazole as standard drugs, all the new pyrimidine and pyrazole derivatives were also evaluated as antimicrobial agents against various gram-positive, gram-negative bacterial and fungal strains.

2. Results and discussion

2.1. Chemistry

The new pyrimidine and pyrazole derivatives were efficiently synthesized as outlined in Scheme 1 starting with compound 2-methoxyaniline **(1)** which was allowed to react with chloroacetonitrile in ethanol leading to the formation of the key intermediate 2-((2-methoxyphenyl) amino) acetonitrile **(2)**. The latter compound **2** was treated with different aromatic aldehydes namely; benzaldehyde and/or 4-methylbenzaldehyde in glacial acetic acid to produce the corresponding acrylonitrile derivatives **3a, b**, which were subsequently reacted with urea and/or thiourea in refluxing ethanol containing a catalytic amount of HCl to afford the pyrimidin-2-ones **4a, b** and pyrimidine-2-thiones **5a, b** respectively. On the other hand, the treatment of **3a, b** with hydrazine hydrate in refluxing ethanol for 8 h accomplished the target pyrazole derivatives **6a, b**. The molecular structures of the new compounds were confirmed depending on their elemental analyses, and spectral data. IR spectra of the target pyrimidine derivatives **4a, b** and **5a, b** showed absorption stretching bands at the regions 3489–3356 cm^{-1} representing NH_2, NH groups, at 1676, 1684 cm^{-1} due to C═O groups of compounds **4a, b** and at 1176, 1159 cm^{-1} representing C═S groups of compounds **5a, b**. On the other hand, ^1H NMR chemical shifts represented the protons of the new pyrimidines **4a, b**, **5a, b** at the expected regions. Singlet signals were presented at δ 3.76–3.85 ppm due to the three protons of $–OCH_3$ functionalities, δ 2.02, 2.15 ppm due to CH_3 protons of compounds **4b**, **5b**, δ 8.36–10.42 representing NH, NH_2 protons as well as the signals of the aromatic protons appeared at their expected regions δ 7.04–8.10 ppm. Also, ^{13}C NMR spectra of the compounds **4a, b**, **5a, b** exhibited singlet signals at the range δ 55.94–58.12 ppm contributing to OCH_3 carbons, δ 17.84, 20.95 ppm due to CH_3 carbons of compounds **4b**, **5b**, as well as at δ 160.27–179.21 ppm for C═O and C═S carbons. Different signals appeared at δ 106.18–153.77 ppm due to the aromatic carbons. Additionally, ^1H NMR spectra of the target pyrazole derivatives **6a, b** represented the methoxy group protons at δ 3.82, 3.78 ppm, the D_2O exchangeable protons of NH_2 and NH at δ 5.76, 6.38, 9.71–12.16 ppm as well as the aromatic protons at δ 7.04–8.08 ppm. Also, ^{13}C NMR spectra of the compounds **6a, b** displayed signals at δ 59.3, 58.15 ppm for OCH_3 carbons, δ 21.88 ppm referring to CH_3 carbon of **6b** and at δ 107.56–147.91 ppm contributing to the aromatic carbons.

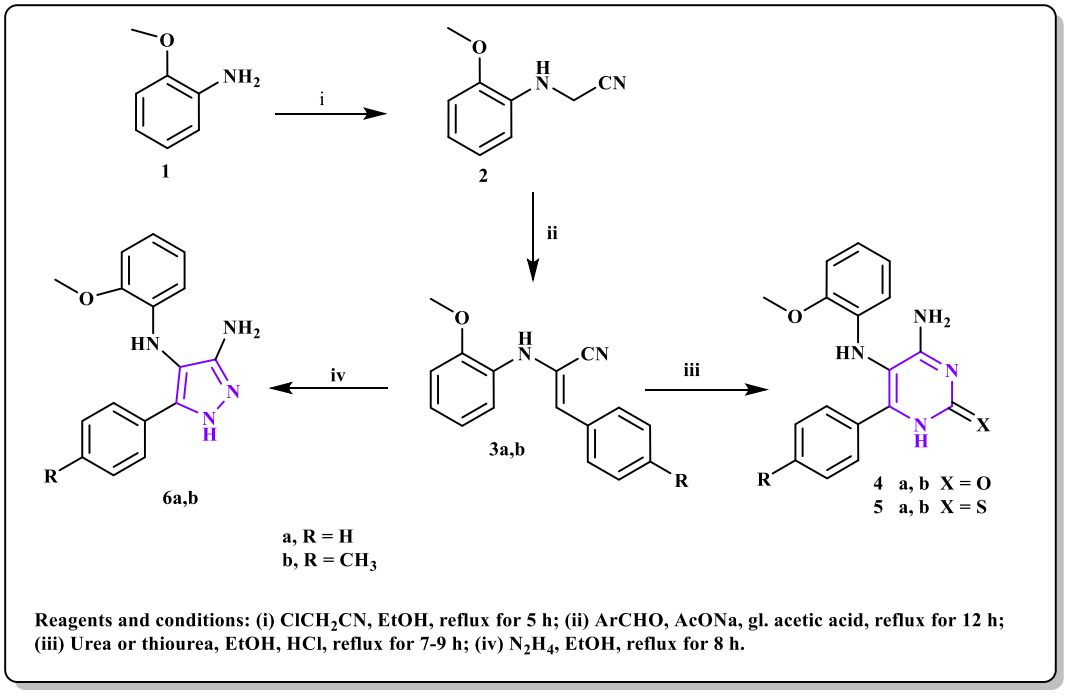

Scheme 1. The synthetic approach for synthesis of the target pyrimidine and pyrazole derivatives.

2.2. Biological activity

2.2.1. In vitro cytotoxic activity

The *in vitro* growth inhibitory potency of the newly prepared compounds was scrutinized against breast (MCF-7) and hepatocellular (HepG-2) cancer cell lines as well as lung fibroblast (WI38) normal cells in comparing with 5-flourouracil and erlotinib as two standard drugs using the colorimetric MTT assay [41,42]. The concentrations of the compounds that induced 50% inhibition of cell viability (IC_{50}, μM) were detected and tabulated in Table 1.

Interestingly, all of the tested derivatives displayed significant cytotoxic activity against both types MCF-7 and HepG2 cancer cell lines of IC_{50} range 0.01–0.35 μM that was much more potent than that obtained by the reference drug erlotinib of IC_{50}; 0.42, 0.82 μM, respectively. On the other hand, while comparing the resultant activities of the compounds with 5-flourouracil, compound 6-phenylpyrimidin-2-one **4a** represented 2 and 3 folds more potent activity than that of the reference drug against MCF-7 and HepG-2 cancer cell lines, respectively (IC_{50}; 0.01 ± 0.03 μM, $IC_{50,\ 5\text{-FU}}$; 0.02 ± 0.01, 0.03 ± 0.01 μM, respectively). A mild decrease in the activity was determined by the analogue 6-(*p*-tolyl) pyrimidin-2-one **4b** to be approximately equipotent to 5-FU of IC_{50}; 0.02 ± 0.01 μM. Further remarkable reduction in the cytotoxic activity was detected by the pyrimidin-2-thione analogues **5a, b** by 2–4 folds against both cancer cell types of IC_{50} values ranging from 0.04 to 0.08 μM. This result could be explained due to the tendency of the pyrimidine-2-oxygen atom to form additional H-bonds with different amino acid residues of the target protein stronger than the sulfur atom [43], thus representing more potent inhibitory effect. Also, the cytotoxic potency was weakened by 4.5–8 folds upon replacement of the pyrimidine moiety with the five-membered pyrazole core as compounds **6a b** exhibiting IC_{50} values ranging from 0.09 ± 0.03–0.16 ± 0.03 μM. Although the key intermediates **2** and **3a, b** represented more potent cytotoxic activity against the tested cell lines comparing to erlotinib as a reference drug, they showed 12–17 folds less cytotoxic activity while comparing to 5-flourouracil of IC_{50} values ranging from 0.24 ± 0.02 to 0.35 ± 0.03 μM. Thus, cyclization of **2** and **3a, b** to establish their pyrimidine and the pyrazole analogues **4a, b–6a, b** is essential to enhance the cytotoxic potency.

Referring to the results of cytotoxicity against WI38 normal cells (Table 1), the nine tested derivatives showed lower cytotoxicity against WI38 (IC_{50}; 39.26–68.01 μM) than 5-FU (IC_{50}; 10 ± 0.056 μM). They exhibited promising safety profile to be safer antitumor agents than the reference drug 5-FU.

2.2.2. Kinase inhibitory assessment

In the present work, the analogues that represented the most potent cytotoxic efficacy were subjected to Kinase inhibitory assessment to investigate their potential mechanism of action. Based on the cytotoxic data, compounds **4a** and **4b** were selected to study their $EGFR^{WT}$, $EGFR^{L858R}$ and $EGFR^{T790M}$ inhibitory activity [44], utilizing erlotinib and osimertinib as standard drugs and the results were expressed as IC_{50} (μM) (Table 2).

Table 1
In vitro cytotoxic efficiency of the new derivatives against MCF-7 as well as HepG-2 cell lines.

Compound No.	IC_{50} (μM)[a]	IC_{50} (μM)[a]	IC_{50} (μM)[a]
	MCF-7	**HePG-2**	**WI-38**
2	0.24 ± 0.02	0.26 ± 0.04	57.31 ± 3.6
3a	0.33 ± 0.01	0.35 ± 0.03	51.32 ± 3.1
3b	0.35 ± 0.02	0.27 ± 0.02	68.01 ± 2.21
4a	0.01 ± 0.03	0.01 ± 0.01	66.27 ± 2.21
4b	0.02 ± 0.01	0.02 ± 0.01	52.08 ± 3.23
5a	0.04 ± 0.04	0.04 ± 0.02	39.98 ± 2.6
5b	0.08 ± 0.02	0.07 ± 0.03	47.75 ± 2.0
6a	0.09 ± 0.03	0.10 ± 0.03	48.75 ± 2.19
6b	0.15 ± 0.01	0.16 ± 0.03	52.32 ± 3.1
5-FU[b]	0.02 ± 0.01	0.03 ± 0.01	10 ± 0.05
Erlotinib	0.42 ± 0.2	0.82 ± 0.4	–

[a] IC50 values = mean ± SD of three independent determinations.
[b] 5-FU: 5-fluorouracil.

Table 2
Inhibitory assessment of the tested compounds **4a** and **4b** in comparison with erlotinib and osimertinib against $EGFR^{WT}$, $EGFR^{L858R}$ and $EGFR^{T790M}$.

Compound No.	IC_{50} (mean ± SEM) (μM)		
	$EGFR^{WT}$	$EGFR^{L858R}$	$EGFR^{T790M}$
Erlotinib	0.096 ± 0.021	0.041 ± 0.20	0.550 ± 0.10
Osimertinib	0.510 ± 0.01	0.020 ± 0.03	0.028 ± 0.05
4a	0.087 ± 0.013	0.044 ± 0.15	0.026 ± 0.01
4b	0.110 ± 0.014	0.058 ± 0.12	0.038 ± 0.04

SEM: Standard error mean; each value is the mean of three values.

Both compounds **4a** and **4b** demonstrated significant $EGFR^{WT}$ inhibitory activity (IC_{50}; 0.087 ± 0.013 and 0.110 ± 0.014 μM) that was approximately equal to that obtained by erlotinib (IC_{50} = 0.096 ± 0.021 μM) and about 5.8 and 4.6 times, respectively higher than that obtained by the reference drug osimertinib (IC_{50} = 0.510 ± 0.011 μM). Furthermore, both compounds **4a** and **4b** employed potent inhibitory activity against $EGFR^{L858R}$ that was close to that obtained by erlotinib (IC_{50} = 0.044 ± 0.15, 0.058 ± 0.12 μM, respectively, $IC_{50,\ Erlotinib}$ = 0.041 ± 0.020), but slightly less than the potency obtained by osimertinib by 2–2.5 folds. Also, 21 and 14 times more significant activity against $EGFR^{T790M}$ was gained by **4a** and **4b**, respectively in comparing to erlotinib (IC_{50} = 0.026 ± 0.15, 0.038 ± 0.12 μM, respectively, $IC_{50,\ Erlotinib}$ = 0.550 ± 0.10) and approximate equal activity while comparing to osimertinib ($IC_{50,\ Erlotinib}$ = 0.028 ± 0.05). Fortunately, both compounds **4a** and **4b** exhibited more potent inhibitory activity against the mutant forms of EGFR over the wild-type form. Taking together, compounds **4a** and **4b** could be considered more advantageous than other EGFR-TKIs since they exhibited promising multi-kinase inhibiting activity (with the highest selectivity toward the mutants $EGFR^{T790M}$ and $EGFR^{L858R}$) that might overcome EGFR-TKIs drug resistance by interfering with intracellular signaling pathways or by suppression the mutated binding sites or genes. Thus, both compounds **4a** and **4b** could be used as promising basic templates for generation of new drugs used for the treatment of different cancer types harboring $EGFR^{T790M}$ and $EGFR^{L858R}$ mutations.

2.2.3. Antimicrobial activity

It has been employed that the pyrimidine and pyrazole motifs are versatile lead molecules in the field of antimicrobial discovery and development [45–47], so it was of interest to assess the antimicrobial activity of the newly prepared compounds alongside their cytotoxic evaluation aiming to gain new pyrimidine and pyrazole candidates of dual potent anticancer and antimicrobial activities. The antimicrobial potency of the tested compounds was *in vitro* screened versus two pathogenic gram-positive bacteria *viz. Streptococcus pneumoniae RCMB 010010* and *Staphylococcus epidermidis RCMB010024*, two pathogenic gram-negative bacteria *viz. Proteus vulgaris RCMB 010085*, *E. Coli RCMB 010052* and two fungal strains *viz. Aspergillus fumigatus RCMB 02568* and *Syncephalastrum racemosum RCMB 05922*. Gentamycin and ketoconazole were utilized as reference drugs for antibacterial and antifungal activity, respectively [48].

The antimicrobial activity of all synthesized compounds was carried out using agar well diffusion method [49] and the obtained results were recorded for each tested compound as the average diameter of the inhibition zones in mm for the bacterial or fungal growth around the discs (Table 3). Furthermore, two-fold serial dilution method [50,51] was utilized to determine the Minimum Inhibitory Concentration (MIC) values (expressed in μg/mL) for the compounds and the results were recorded in (Table 4).

Table 3
In vitro antimicrobial activities of the synthesized compounds using well diffusion agar assay and expressed as mean diameter of inhibition zones (mm)

Compd. No.	Mean diameter of inhibition zones (Mean ± SEM) (mm)					
	Gram + ve Bacteria		**Gram-ve Bacteria**		**Fungi**	
	Streptococcus pneumoniae RCMB 010,010	***Staphylococcus epidermidis RCMB010024***	***Proteus vulgaris RCMB 010,085***	***E. coliRCMB 010,052***	**Aspergillus fumigatus RCMB 02,568**	***SyncephalastrumracemosumRCMB 05,922***
2	16.4 ± 0.16	NA	14.3 ± 0.24	11.2 ± 0.14	NA	NA
3a	NA	13.9 ± 0.29	18.4 ± 0.36	NA	NA	NA
3b	NA	NA	NA	NA	NA	NA
4a	27.0 ± 0.11	25.1 ± 0.15	19.7 ± 0.14	25.3 ± 0.18	22.8 ± 0.17	18.9 ± 0.50
4b	25.0 ± 0.33	24.5 ± 0.14	18.6 ± 0.15	26.2 ± 0.01	22.2 ± 0.10	20.3 ± 0.14
5a	23.2 ± 0.15	21.9 ± 0.26	17.3 ± 0.43	24.1 ± 0.13	21.4 ± 0.12	19.1 ± 0.22
5b	19.8 ± 0.24	20.1 ± 0.18	16.5 ± 0.13	18.2 ± 0.44	12.1 ± 0.18	16.2 ± 0.46
6a	15.5 ± 0.32	10.8 ± 0.16	13.7 ± 0.16	12.1 ± 0.25	17.1 ± 0.15	21.7 ± 0.15
6b	18.6 ± 0.15	NA	NA	22.0 ± 0.14	NA	NA
Gentamycin	27.2 ± 0.80	25.4 ± 0.180	19.9 ± 0.30	26.3 ± 0.15	–	–
Ketoconazole	–	–	–	–	23.7 ± 0.10	22.8 ± 0.10

NA: No activity under the screening conditions; -: Not tested; SEM = standard error mean; each value is the mean of different values.

Table 4
Minimal inhibitory concentrations (MICs) of the synthesized compounds against the tested pathogenic bacteria and fungi.

Compound No.	MIC (Mean ± SEM) (μg/mL)					
	Gram + ve Bacteria		**Gram -ve Bacteria**		**Fungi**	
	Streptococcus pneumoniae RCMB 010,010	***Staphylococcus epidermidis RCMB010024***	***Proteus vulgaris RCMB 010,085***	***E. ColiRCMB 010,052***	**Aspergillus fumigatus RCMB 02,568**	***Synce-phalastrumracemosum RCMB 05,922***
2	31.25 ± 0.50	NA	125 ± 0.72	500 ± 0.83	NA	NA
3a	NA	125 ± 0.25	7.81 ± 0.11	NA	NA	NA
4a	0.03 ± 0.55	0.06 ± 0.32	0.98 ± 0.35	0.06 ± 0.15	0.12 ± 0.45	0.98 ± 0.62
4b	0.06 ± 0.11	0.06 ± 0.22	7.81 ± 0.27	0.03 ± 0.25	0.49 ± 0.11	0.98 ± 0.17
5a	0.12 ± 0.33	0.49 ± 0.09	15.63 ± 0.76	0.12 ± 0.28	0.24 ± 0.18	31.25 ± 0.34
5b	0.98 ± 0.22	1.95 ± 0.35	31.25 ± 0.45	62.5 ± 0.78	250 ± 0.92	31.25 ± 0.34
6a	62.5 ± 0.11	500 ± 0.53	125 ± 0.85	250 ± 0.37	7.81 ± 0.71	0.24 ± 0.05
6b	7.81 ± 0.13	NA	NA	0.49 ± 0.70	NA	NA
Gentamycin	0.24 ± 0.66	0.06 ± 0.72	1.95 ± 0.15	0.03 ± 0.82	–	–
Ketoconazole	–	–	–	–	0.12 ± 0.68	0.49 ± 0.07

On the basis of the MIC values in Table 4, it was exhibited that there is a wide variability in the antimicrobial potency of the tested derivatives. It has been detected that the pyrimidine-2-one derivatives **4a** and **4b** were 8–6 folds more potent antibacterial candidates against ***Streptococcus pneumoniae*** (MIC; 0.03, 0.06 μg/mL) than gentamicin (MIC; 0.24 μg/mL). Also, they were equipotent to the reference drug gentamicin against ***Staphylococcus epidermidis*** exhibiting MIC values; 0.06 μg/mL. Furthermore, both **4a** and **4b** represented approximate equal potency to that obtained by gentamicin against both tested gm-negative bacteria ***Proteus vulgaris*** and ***E. Coli*** (MIC values; 0.98, 0.06, 0.03 μg/mL) (MIC $_{\text{Gentamycin}}$; 1.95, 0.03 μg/mL). Compound **4b** was **4** folds less potent than gentamicin against ***E. Coli*** of MIC value; 7.81 μg/mL. On the other hand, the antifungal activity of the **4a** and **4b** was slightly less than that of the reference drug Ketoconazole representing MIC values ranging from 0.12 to 0.98 μg/mL, MIC $_{\text{Ketoconazole}}$; 0.12, 0.49 μg/mL.

Conversely, the pyrimidine-2-thione derivatives **5a** and **5b** appeared to be less potent as antibacterial agents against the tested gm-positive of MIC values range 0.49–1.95 μg/mL except compound **5a** which represented more potent activity against *Streptococcus pneumoniae RCMB 010010* of MIC value 0.12 μg/mL, while comparing to gentamicin. Unfortunately, both **5a** and **5b** exhibited moderate activity against the tested gm-negative bacteria of MIC range; 0.12–62.5 μg/mL and moderate to weak potency against the tested fungal strains of MIC range; 31.25–250 μg/mL, comparing to Ketoconazole.

Depending on the resultant data the pyrimidine-2-one is a promising scaffold in producing antibacterial activity more than pyrimidine-2-thione nucleus.

2.3. Computational studies

2.3.1. Molecular docking

To furnish a deep insight into the binding modes of the most potent new derivatives **4a** and **4b** within the active sites of $EGFR^{WT}$ and $EGFR^{T790M}$ enzymes, molecular docking simulation was done using Molecular Operating Environment software (MOE®) 2008.10 [52]. MOE program. Validation of the docking procedures were firstly done via re-docking of the original co-crystallized ligands, erlotinib and AZD9291 within the active sites of $EGFR^{WT}$ and $EGFR^{T790M}$ enzymes (PDB code: 1 M17 and 6JX0) and revealed energy scores −12.25 and −11.75 kcal/mol at root mean square deviation (RMDS) values equal 0.75 and 0.88 Å, respectively [53,54].

The docking results of **4a** and **4b** within the ATP-binding pocket of $EGFR^{WT}$ illustrated that they interact with $EGFR^{WT}$ through similar hydrogen bonding interactions with energy scores of −13.22 and −12.90 kcal/mol, respectively. The 4-aminopyrimidine-2-one ring was fitted through H-bond acceptors between the carbonyl oxygen and the backbone of the key amino acid Met769 (distance in **4a** and **4b**: 2.88 and 2.58 Å, respectively). The protons of the amino groups formed H-bond donors with the sidechain of Gln767 in case of **4a** and **4b** (distance: 1.66 and 2.21 Å, respectively) and additional H-bond donor with the sidechain of Gln766 in case of **4a** (distance: 2.38 Å). Moreover, the side chain of Thr766 afforded two H-bonds with the proton of NH and the oxygen of methoxy group (Figs. 4 and 5).

On the other hand, the promising targets **4a** and **4b** bound nicely within the ATP-active site of $EGFR^{T790M}$ in a similar manner with energy scores of −12.65 and −11.88 kcal/mol, respectively. The 4-

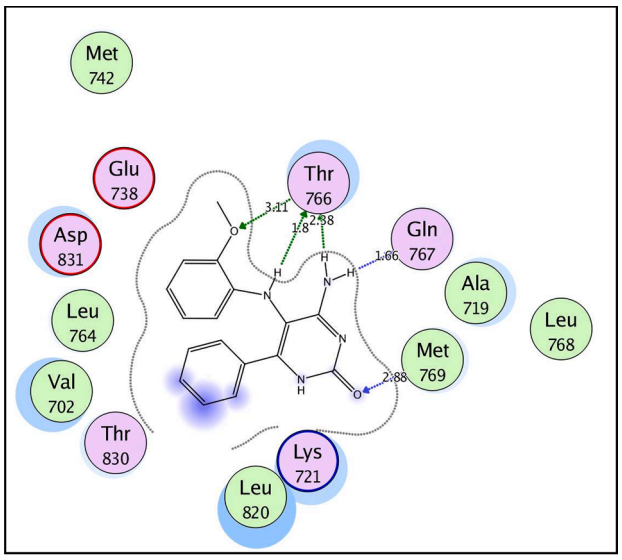

A

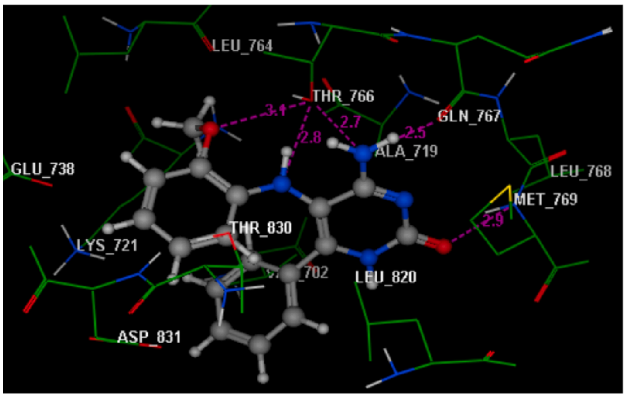

B

Fig. 4. A & B images representing 2D & 3D binding views of compound **4a** into the active site of EGFR^{WT} (PDB ID: 1 M17).

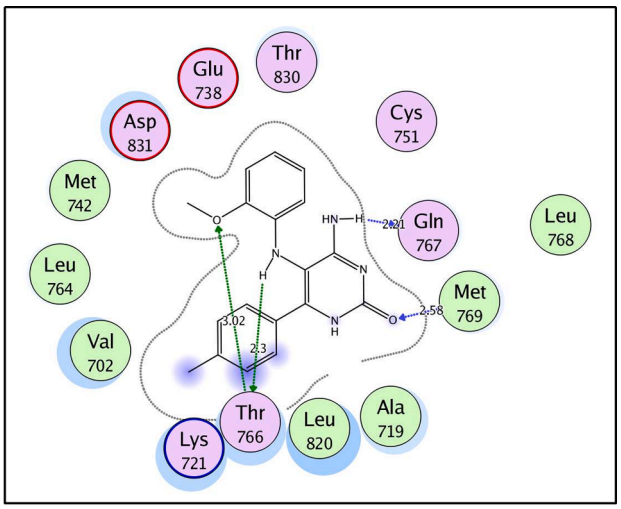

A

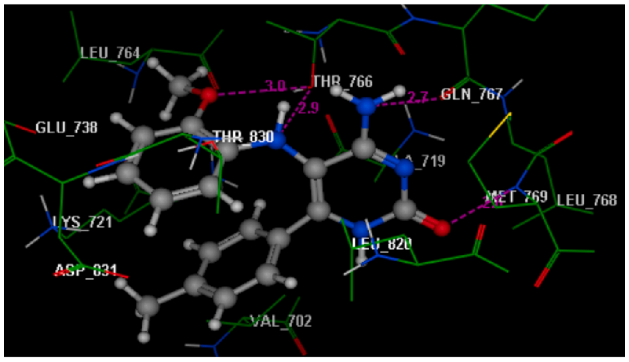

B

Fig. 5. A & B images representing 2D & 3D binding views of compound **4b** into the active site of EGFR^{WT} (PDB ID: 1 M17).

aminopyrimidine-2one scaffold was fixed tightly via two hydrogen bond donors between N-3 and the carbonyl oxygen with the backbone of **Met793**. Furthermore, the proton of the amino group exhibited H-bond donors with the backbone of **Gln791** in case of **4a** and **4b** (distance: 1.87 and 1.65 Å, respectively) **(**Figs. 6 and 7**)**.

Finally, and referring to the superimposition models in Fig. 8, the two compounds **4a** and **4b** bearing 4-aminopyrimidine-2-one scaffold were well embedded in the active pockets of EGFR^{WT} and EGFR^{T790M} through various H-bond interactions. Furthermore, the illustrated binding pattern explained the excellent EGFR^{WT} and EGFR^{T790M} inhibitory activity of these derivatives comparing with the co-crystalized inhibitors erlotinib and AZD9291, respectively.

2.3.2. *In silico ADMET prediction and drug likeness study*

Based on the Lipinski's rule (Rule of five) using molinspiration software [55,56] **(**Table 5**)**, all tested compounds satisfy the "Rule of five" and meet all criteria for good permeability and bioavailability displaying rotatable bonds number in the range of 3–4, with the lowest value allowed to compound **2**, therefore, obviously exhibiting small conformational flexibility. The percentage of absorption (%ABS) which is deduced from the TPSA values according to the following equation: % ABS = 109–0.345 × TPSA was also determined. All candidate compounds exhibited a great %ABS ranging from 76.90 to 93.45% suggesting their efficient oral absorption. Topological polar surface area (TPSA) results are < 140 Å2 for all the analyzed compounds suggesting that they are candidates for good solubility, capacity for penetrating cell membranes and intestinal absorption and are basically recognized as good indicators of drug transport in the intestines, Caco-2 monolayers penetration, and blood-brain barrier crossing [56–58]. Their nOHNH value (H-bond donors) are less than 5 giving them higher solubility in cellular membranes with also nON values (H-bond acceptors) in the range of 3–6 and molecular weight in the range of 162.19–338.44. Molecular volumes of the target compounds in this series increased as increasing MW and ranged from 155.65 to 301.35 Å3. The milog P (octanol/water partition coefficient) values for all compounds under inspection are less than 5, especially for compounds **2**, **4a** and **4b** outlining them a good lipophilicity character. The great lipophilicity of these compounds may protect against ROS (Reactive Oxygen species) damage and is due in part to their smaller polar surface areas.

2.3.2.1. In silico toxicity potential. Toxicity risks and physicochemical properties of the newly synthesized compounds were estimated via the methodology developed by Osiris [59]. All compounds were predicted for their toxicity including mutagenicity, tumorgenicity, skin irritancy and reproductive effect. From the results displayed in Table 6, all compounds would be safe and were predicted to have no side effects. The best results were obtained by compounds **4a**, **4b**, **5a**, **5b**, **6a** and **6b** indicating that they contain predominantly active fragments which are frequently presented in commercial drugs [60]. Drug score is a measure of compound's potential to have drug-conform behavior. The highest drug-score value was ascribed to compound **4a** justifying its both effectiveness and potentiality as a new drug candidate.

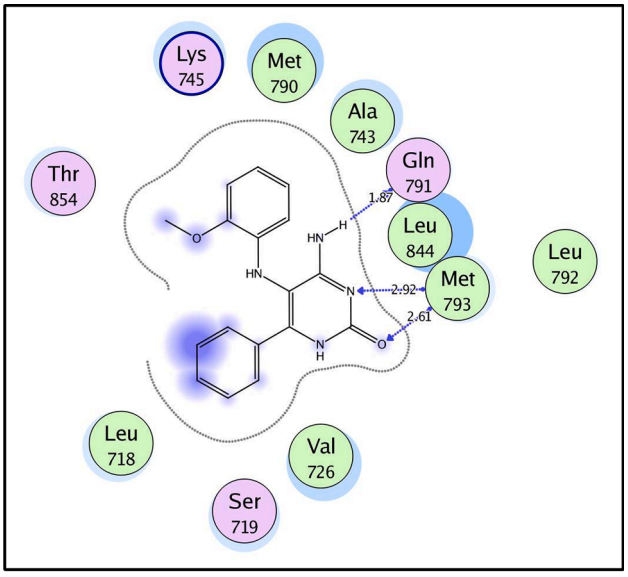

A

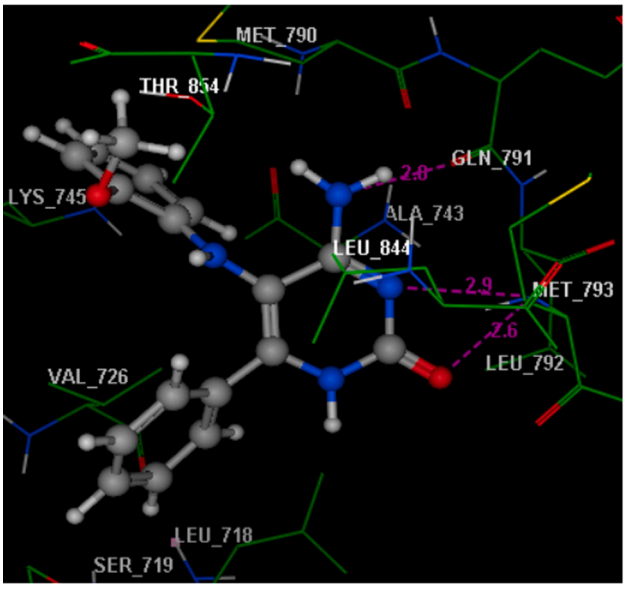

B

Fig. 6. A & B images representing 2D & 3D binding views of compound **4a** into the active site of $EGFR^{T790M}$ (PDB ID: 6JX0).

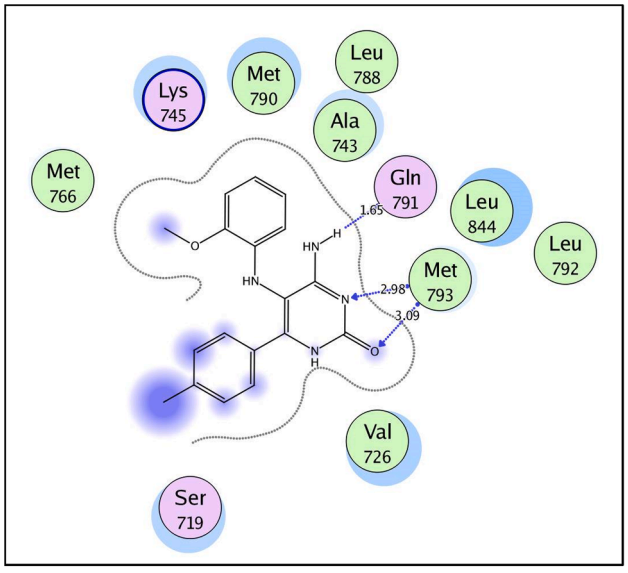

A

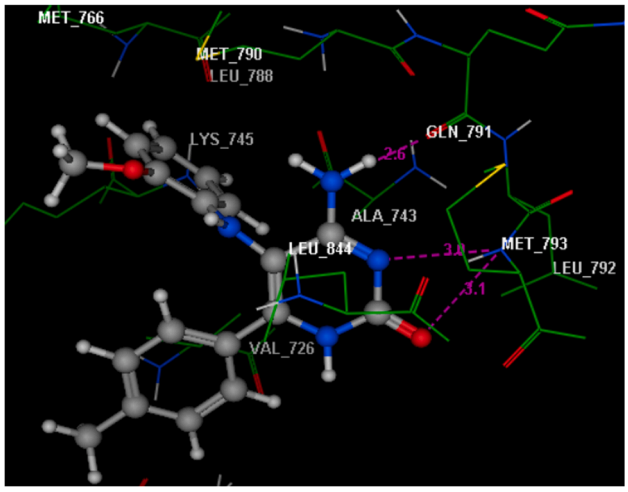

B

Fig. 7. A & B images representing 2D & 3D binding views of compound **4b** into the active site of $EGFR^{T790M}$ (PDB ID: 6JX0).

3. Conclusions

In summary, new pyrimidine-2-one(thione) and pyrazole derivatives bearing the essential pharmacophoric features of EGFR-TKIs were designed, synthesized and evaluated as cytotoxic candidates against human breast (MCF-7) and hepatocellular (HepG2) cancer cell lines, where 5-flourouracil and erlotinib were serving as standard drugs. All the new compounds revealed more potent cytotoxic activity than erlotinib. On the other hand, only the pyrimidine-2-one compound **4a** exhibited more potent anticancer activity than 5-flourouracil, while **4b** analogue was equipotent to it. The inhibitory profiles against the three isoforms $EGFR^{WT}$, $EGFR^{L858R}$ and $EGFR^{T790M}$ were evaluated for the most promising compounds **4a**, **4b,** utilizing erlotinib and osimertinib as reference drugs. Both analogues **4a**, **4b** exhibited more potent suppression effect against the mutant forms $EGFR^{L858R}$ and $EGFR^{T790M}$ over the wild-type form $EGFR^{WT}$ and hence they might overcome resistance to EGFR-TKIs. Molecular docking study rationalized the potent suppression effect of the pyrimidine −2-ones **4a** and **4b** due to their good fitting with the best binding energy in the active site of $EGFR^{WT}$ and its mutated isoforms $EGFR^{L858R}$ and $EGFR^{T790M}$. As a trial to gain new pyrimidine and pyrazole – based derivatives of dual anticancer and antimicrobial activity, all the new analogues were assessed as antibacterial and antifungal agents against a number of pathogenic gram-positive, gram-negative bacterial and fungal strains using gentamycin and ketoconazole as standard drugs. The results proved that **4a** and **4b** among the tested derivatives were the most promising agents representing a wide spectrum antimicrobial activity against the examined microbes. Furthermore, Lipinski rule of five and ADME profile suggested strongly that all the synthesized pyrazole and pyrimidine compounds were fulfilling the criteria of drug likeness approach. Accordingly, the pyrimidine scaffold is considered as a promising template in the field of development and optimization of new drugs of dual anticancer and antimicrobial activities.

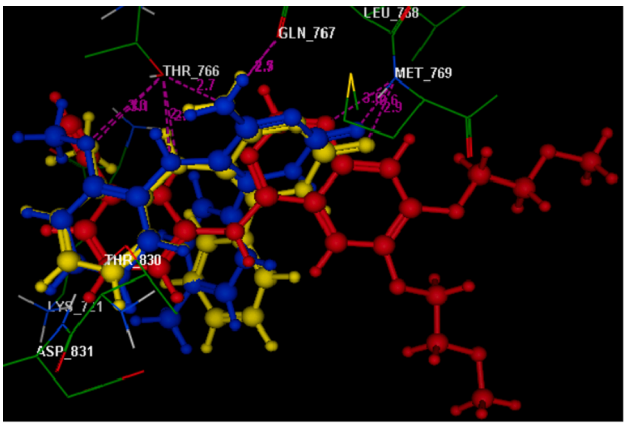

A

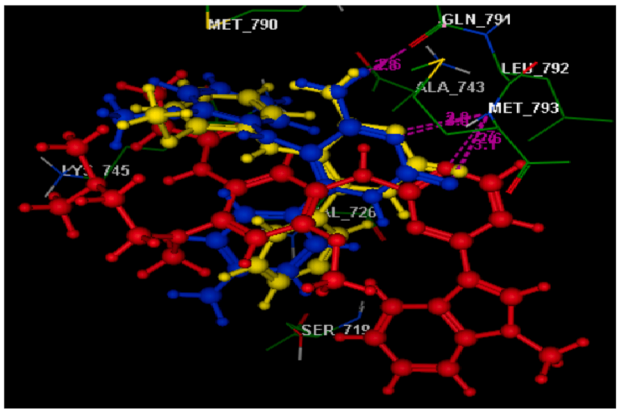

B

Fig. 8. 3D superimposition binding views of compound **4a** (yellow) and **4b** (blue) with erlotinib (red) into the active site of $EGFR^{WT}$ (PDB ID: 1 M17) (A) and with AZD9291 (red) into the active site of $EGFR^{T790M}$ (PDB ID: 6JX0) (B), respectively. (For interpretation of the references to colour in this figure legend, the reader is referred to the web version of this article.)

4. Experimental

4.1. Chemistry

The instruments used for measuring the melting points, spectral data (IR, Mass, ^{1}H NMR and ^{13}C NMR) and elemental analysis are provided in details in Supplementary material.

4.1.1. 2-((2-Methoxyphenyl) amino) acetonitrile (2)

A mixture of 2-methoxyaniline (**1**) (1.2 g, 10 mmol) and chloroacetonitrile (0.75 g, 10 mmol) in absolute ethanol (20 mL) was refluxed for 5 h. The solid product formed after cooling was collected by filtration and recrystallized from ethanol to afford the title compound **2**.

Yield 82%, colorless; m.p. 160-162℃; IR (ν_{max}/cm^{-1}): 3328 (NH), 3039 (CH-arom.), 2972 (CH-aliph.), 2223 (CN), 1602 (C═C); ^{1}H NMR (DMSO-d_6): δ 3.85 (s, 3H, OCH_3), 4.53 (s, 2H, CH_2), 7.17–7.37 (m, 3H, Ar-H), 7.53 (d, 1H, J = 10.00 Hz, Ar-H), 9.43 (s, 1H, NH, D_2O exchangeable); ^{13}C NMR (DMSO-d_6): δ 48.20 (–CH_2), 56.19 (OCH_3), 112.77, 115.32, 116.82, 120.09, 123.99, 136.43; Anal. for $C_9H_{10}N_2O$ (162.19): Calcd. C, 66.65; H, 6.21; N, 17.27; Found: C, 66.87; H, 6.43; N, 17.49%.

4.1.2. General procedure for the synthesis of 2-((2-methoxyphenyl) amino)-3-(substituted) acrylonitrile 3a, b

A mixture of the acetonitrile derivative **2** (1.6 g, 10 mmol), appropriate aromatic aldehydes namely; benzaldehyde and/or 4-methylbenzaldehyde (10 mmol) and anhydrous sodium acetate (10 mmol) in glacial acetic acid (15 mL) was refluxed for 12 h then allowed to cool. The solid product was collected, dried and recrystallized from dioxane.

4.1.2.1. 2-((2-Methoxyphenyl) amino)-3-phenylacrylonitrile (3a). Yield 71%; brown crystals; m.p. 222-224℃; IR (ν_{max}/cm^{-1}): 3374 (NH), 3035 (CH-arom.), 2967 (CH-aliph.), 2222 (CN), 1611 (C═C); ^{1}H NMR (DMSO-d_6): δ 3.75 (s, 3H, OCH_3), 7.33–7.37 (m, 2H, Ar-H), 7.54–7.57 (m, 2H, Ar-H), 7.64–7.66 (m, 3H, Ar-H), 8.19 (d, 2H, J = 10.00 Hz, Ar-H), 8.34 (s, 1H, -C = CH), 9.87 (s, 1H, NH, D_2O exchangeable); ^{13}C NMR (DMSO-d_6): δ 56.36 (OCH_3), 111.45, 113.27, 115.57, 117.85, 120.05, 122.79, 123.69, 125.12, 126.97, 127.80, 132.44, 136.35, 141.80; Anal. for $C_{16}H_{14}N_2O$ (250.30): Calcd. C, 76.78; H, 5.64; N, 11.19; Found: C, 76.55; H, 5.86; N, 11.41.

Table 5
Calculated molecular properties of the newly synthesized compounds for assessment of the drug likeness.

Compd No.Rule	m_iLogP[a]<5	% ABS[b]	TPSA[c]	N_{atoms}[d]	MW[e]<500	M.Vol.[f]	n_{ON}[g]<10	n_{OHNH}[h] [g]<5	$n_{viol.}$[i]	n_{rotb}[j](<10)
2	1.59	93.45	45.05	12	162.19	155.65	3	1	0	3
3a	4.05	93.45	45.05	19	250.30	237.68	3	1	0	4
3b	4.50	93.45	45.05	20	264.33	254.24	3	1	0	4
4a	3.08	76.90	93.04	23	308.34	275.91	6	4	0	4
4b	3.53	76.90	93.04	24	322.37	292.47	6	4	0	4
5a	3.42	82.79	75.97	23	324.41	284.79	5	4	0	4
5b	3.87	82.79	75.97	24	338.44	301.35	5	4	0	4
6a	3.53	82.79	75.97	21	280.33	256.93	5	4	0	4
6b	3.98	82.79	75.97	22	294.36	273.49	5	4	0	4
Gentamycin	−4.21	40.08	199.74	33	477.60	450.66	12	11	2	7
Ketoconazole	3.77	85.16	69.08	36	531.44	452.47	8	0	1	7
5-FU	−0.59	86.32	65.72	9	130.08	96.91	4	2	0	0

[a] Octanol-water partition coefficient, calculated by the methodology developed by Molinspiration.
[b] % ABS: percentage of absorption.
[c] TPSA topological polar surface area.
[d] Number of non-hydrogen atoms.
[e] Molecular weight.
[f] molecular volume.
[g] Number of hydrogen-bond acceptors (O and N atoms).
[h] Number of hydrogen-bond donors (OH and NH groups).
[i] Number of "Rule of five" violations
[j] Number of rotatable bonds.

Table 6
Toxicity risks, solubility, drug-likeness, and drug score of the synthesized compounds.

Compound No.	Toxicity risks				Solubility	Drug-likeness	DrugScore
	Mutagen-icity	Tumorigen-icity	Irritancy	Reproductive effect			
2	green	green	green	green	−2.14	−3.72	0.49
3a	green	green	green	green	−4.12	−4.36	0.39
3b	green	green	green	green	−4.46	−4.69	0.35
4a	green	green	green	green	−3.93	2.24	0.78
4b	green	green	green	green	−4.27	1.01	0.67
5a	green	green	green	green	−4.01	1.33	0.72
5b	green	green	green	green	−4.35	0.11	0.57
6a	green	green	green	green	−4.16	2.60	0.76
6b	green	green	green	green	−4.51	1.35	0.66
Gentamycin	green	green	green	green	−1.18	4.88	0.77
Ketoconazole	green	green	green	green	−2.99	11.18	0.61
5-FU	red	red	red	red	−1.76	−4.50	0.06

Green; low risk, red: high risk

4.1.2.2. 2-((2-Methoxyphenyl) amino)-3-(p-tolyl) acrylonitrile (3b). Yield 68%; brown crystals; m.p. 217-219℃; IR (ν_{max}/cm^{-1}): 3279 (NH), 3062 (CH-arom.), 2933 (CH-aliph.), 2205 (CN) 1602 (C═C); ^{1}H NMR (DMSO-d_6): δ 2.01 (s, 3H, CH_3), 3.86 (s, 3H, OCH_3), 7.11–7.18 (m, 2H, Ar-H), 7.27–7.32 (m, 1H, Ar-H), 7.47 (d, 1H, J = 10.00 Hz, Ar-H), 7.84 (d, 2H, J = 10.00 Hz, Ar-H), 7.99 (d, 2H, J = 10.00 Hz, Ar-H), 8.26 (s, 1H, -C = CH), 9.65 (s, 1H, NH, D_2O exchangeable); ^{13}C NMR (DMSO-d_6): δ 20.08 (CH_3), 55.23 (OCH_3), 111.81, 112.90, 114.81, 116.43, 120.85, 121.02, 122.36, 127.37, 129.71, 130.74, 132.42, 135.58, 139.90, 143.80; Anal. for $C_{17}H_{16}N_2O$ (264.32): Calcd. C, 77.25; H, 6.10; N, 10.60; Found: C, 77.46; H, 6.31; N, 10.82.

4.1.3. General procedure for the preparation of 4-amino-5-((2-methoxyphenyl) amino)-6-(substituted phenyl) pyrimidin-2(1H)-one (thione) derivatives 4a, b and 5a, b

A mixture of the compounds **3a, b** (10 mmol), urea and/ or thiourea (10 mmol) in absolute ethanol (20 mL) containing (1 mL) hydrochloric acid was heated under reflux for 7–9 h. The solid product produced on hot was collected by filtration and recrystallized from ethanol to give the target products **4a, b** and **5a, b**, respectively.

4.1.3.1. 4-Amino-5-((2-methoxyphenyl) amino)-6-phenylpyrimidin-2 (1H)-one (4a). Yield 63%; yellow crystals; m.p. 276-278℃; IR (ν_{max}/cm^{-1}): 3445, 3356 (NH_2), 3282, 3180 (2NH), 3086 (CH-arom.), 2973 (CH-aliph.), 1676 (C═O), 1621 (C═C); ^{1}H NMR (DMSO-d_6): 3.76 (s, 3H, OCH_3), 7.41–7.45 (m, 4H, Ar-H, NH_2, D_2O exchangeable), 7.55–7.75 (m, 5H, Ar-H), 8.14 (d, 2H, J = 10.00 Hz, Ar-H), 9.07, 10.2 (2 s, 2H, 2NH, D_2O exchangeable); ^{13}C NMR (DMSO- d_6): δ 57.87 (OCH_3), 108.89, 110.75, 113.88, 116.41, 122.22, 122.39, 125.16, 127.9, 128.60, 133.76, 136.71, 153.77, 160.27 (C═O); Anal. for $C_{17}H_{16}N_4O_2$ (308.33): Calcd. C, 66.22; H, 5.23; N, 18.17; Found: C, 66.45; H, 5.43; N, 18.38.

4.1.3.1.1. 4-Amino-5-((2-methoxyphenyl) amino)-6-(p-tolyl) pyrimidin-2(1H)-one (4b). Yield: 66%; yellow crystals; m.p. 263-265℃; IR (ν_{max}/cm^{-1}): 3466, 3386 (NH_2), 3298, 3170 (2NH), 3055 (CH-arom.), 2969 (CH-aliph.), 1684 (C═O), 1609 (C═C); ^{1}H NMR (DMSO-d_6): 2.15 (s, 3H, CH_3), 3.85 (s, 3H, OCH_3), 7.15–7.33 (m, 4H, Ar-H, NH_2, D_2O exchangeable), 7.48 (d, 1H, J = 10.00 Hz, Ar-H), 7.82 (d, 1H, J = 10.00 Hz, Ar-H), 8.01 (d, 2H, J = 10.00 Hz, Ar-H), 8.27 (d, 2H, J = 10.00 Hz, Ar-H), 9.72, 10.39 (2 s, 2H, 2NH, D_2O exchangeable); ^{13}C NMR (DMSO-d_6): δ 17.84 (CH_3), 55.94 (OCH_3), 106.18, 109.12, 111.84, 116.34, 121.96, 122.06, 125.19, 129.15, 130.64, 134.24, 137.72, 142.13, 153.64, 161.24 (C═O); Anal. for $C_{18}H_{18}N_4O_2$ (322.36): Calcd. C, 67.07; H, 5.63; N, 17.38; Found: C, 67.28; H, 5.85; N, 17.59.

4.1.3.2. 4-Amino-5-((2-methoxyphenyl) amino)-6-phenylpyrimidine-2 (1H)-thione (5a). Yield 71%; yellow crystals; m.p. 287-289℃; IR (ν_{max}/cm^{-1}): 3432, 3379 (NH_2), 3271, 3108 (2NH), 3042 (CH-arom.), 2924 (CH-aliph.), 1607 (C═C), 1176 (C═S); ^{1}H NMR (DMSO-d_6): δ 3.77 (s, 3H, OCH_3), 7.23–8.01 (m, 9H, Ar-H), 8.36 (s, 2H, NH_2, D_2O exchangeable), 9.92, 10.42 (2 s, 2H, 2NH, D_2O exchangeable); ^{13}C NMR (DMSO-d_6): δ 56.28 (OCH_3), 106.14, 109.20, 115.32, 121.01, 122.32, 124.98, 126.41, 127.62, 129.85, 134.25, 136.30, 141.84, 151.45, 178.21 (C═S); Anal. for $C_{17}H_{16}N_4OS$ (324.40): Calcd. C, 62.94; H, 4.97; N, 17.27; S, 9.88; Found: C, 62.73; H, 4.75; N, 17.48; S, 9.67.

4.1.3.3. 4-Amino-5-((2-methoxyphenyl) amino)-6-(p-tolyl) pyrimidine-2 (1H)-thione (5b). Yield 69%; yellow crystals; m.p. 291-293℃; IR (ν_{max}/cm^{-1}): 3489, 3369 (NH_2), 3244, 3153 (2NH), 3043 (CH-arom.), 2930 (CH-aliph.), 1159 (C═S); ^{1}H NMR (DMSO-d_6): 2.02 (s, 3H, CH_3), 3.85 (s, 3H, OCH_3), 7.11 (d, 2H, J = 10.00 Hz, Ar-H), 7.20–7.60 (m, 6H, Ar-H), 7.89 (s, 2H, NH_2, D_2O exchangeable), 9.16, 9.94 (2 s, 2H, 2NH, D_2O exchangeable); ^{13}C NMR (DMSO-d_6) δ: 20.95 (CH_3), 58.12 (OCH_3), 105.80, 110.12, 117.74, 121.64, 123.77, 125.09, 127.65, 128.79, 130.79, 133.72, 136.42, 142.35, 153.78, 179.11 (C═S); Anal. for $C_{18}H_{18}N_4OS$ (338.43): Calcd. C, 63.88; H, 5.36; N, 16.56; S, 9.47; Found: C, 63.65; H, 5.58; N, 16.75; S, 9.68.

4.1.4. General procedure for the preparation of compounds N^4-(2-methoxyphenyl)-5-substituted phenyl-1H-pyrazole-3,4-diamine derivatives 6a, b

A mixture of compounds **3a, b** (10 mmol) and hydrazine hydrate (2 mL) in ethanol (30 mL) was refluxed for 8 h. After cooling, the obtained precipitate was filtered, dried and crystallized from dioxane to give the corresponding derivatives **6a, b**.

4.1.4.1. N^4-(2-Methoxyphenyl)-5-phenyl-1H-pyrazole-3,4-diamine (6a). Yield 59%; brown crystals; m.p. 300-302℃; IR (ν_{max}/cm^{-1}): 3481, 3308 (NH_2), 3278, 3155 (2NH), 3063 (CH-arom.), 2925 (CH-aliph.), 1607 (C═C); ^{1}H NMR (DMSO-d_6): 3.82 (s, 3H, OCH_3), 5.76 (s, 2H, NH_2, D_2O exchangeable), 7.04–7.10 (m, 2H, Ar-H), 7.35–7.45 (m, 2H, Ar-H), 7.55–7.62 (m, 3H, Ar-H), 7.85 (d, 2H, Ar-H, J = 10.00 Hz), 9.71, 12.16 (s, 2H, 2NH, D_2O exchangeable); ^{13}C NMR (DMSO- d_6): δ 59.3 (OCH_3), 107.56, 112.03, 115.03, 120.77, 123.27, 125.18, 127.87, 128.35, 131.24, 134.75, 139.88, 141.25, 147.91. Anal. for $C_{16}H_{16}N_4O$ (280.32): Calcd. C, 68.55; H, 5.75; N, 19.99; Found: C, 68.76; H, 5.93; N, 19.77.

4.1.4.2. N^4-(2-Methoxyphenyl)-5-(p-tolyl)-1H-pyrazole-3,4-diamine (6b). Yield 56%; brown crystals; m.p. 296-298℃; IR (ν_{max}/cm^{-1}): 3428, 3332 (NH_2), 3185, 3129 (2NH), 3032 (CH-arom.), 2966, 2912 (CH-aliph.), 1620 (C═C); ^{1}H NMR (DMSO-d_6): 2.31 (s, 3H, CH_3), 3.78 (s, 3H, OCH_3), 6.38 (s, 2H, NH_2, D_2O exchangeable), 7.07 (d, 1H, J = 10.00 Hz, Ar-H), 7.43–7.74 (m, 3H, Ar-H), 7.99 (d, 2H, J = 10.00 Hz, Ar-H), 8.08 (d, 2H, J = 10.00 Hz, Ar-H), 9.98, 12.30 (2 s, 2H, 2NH, D_2O exchangeable); ^{13}C NMR (DMSO- d_6): δ 21.88 (CH_3), 58.15 (OCH_3), 111.92, 113.90, 115.81, 120.65, 120.71, 123.96, 126.40, 129.48, 130.35, 132.57, 138.15, 143.21, 147.87; Anal. for $C_{17}H_{18}N_4O$ (294.35):

Calcd. C, 69.37; H, 6.16; N, 19.03; Found: C, 69.55; H, 6.37; N, 19.25.

4.2. *In vitro anticancer screening*

The screening was performed using MTT assay [41,42] at Regional Center for Mycology and Biotechnology, Al- Azhar University. More details were provided in Supplementary material.

4.3. *$EGFR^{WT}$, $EGFR^{L858R}$ and $EGFR^{T790M}$ kinase inhibitory assay*

Homogeneous time resolved fluorescence (HTRF) assay was applied [44]. More details were provided in Supplementary material.

4.4. *Antimicrobial activity assay*

In vitro microbial activities were carryout at the Regional Center for Mycology and Biotechnology (RCMB), Al-Azhar University, Cairo, Egypt. Agar plate diffusion technique was used [49]. More details were provided in Supplementary material.

4.5. *Minimal inhibitory Concentration (MIC) measurement*

The bacteriostatic activity of the compounds was then evaluated using the two-fold serial dilution technique [50,51]. More details were provided in Supplementary material.

4.6. *Molecular modeling studies*

Three-dimensional structures of the newly synthesized active EGFR inhibitors **4a** and **4b** in their neutral forms were drawn using Molecular Operating Environment software (MOE®) 2008.10 [52–54]. More details were provided in Supplementary material.

4.7. *In silico ADMET analysis*

ADMET descriptors (absorption, distribution, metabolism, excretion and toxicity) of the compounds were determined using molinspiration software. The tested compounds were prepared and the energy was minimized according to the preparation using the small molecule protocol. Then the ADMET descriptor protocol was applied to calculate the different descriptors [59,60].

Declaration of Competing Interest

The authors declare that they have no known competing financial interests or personal relationships that could have appeared to influence the work reported in this paper.

Acknowledgments

The authors are thankful to the Faculty of Pharmacy-Al-Azhar University / Egypt, for performing the spectral and biological data of the new target compounds.

Appendix A. Supplementary data

Supplementary data to this article can be found online at https://doi.org/10.1016/j.bioorg.2021.105078.

References

[1] M.A. Abdelgawad, R.B. Bakr, O.A. Alkhoja, W.R. Mohamed, Design, synthesis and antitumor activity of novel pyrazolo[3,4-d] pyrimidine derivatives as EGFR-TK inhibitors, Bioorg. Chem. 66 (2016) 88–96.
[2] J.M.d. Akhtar, A.A. Khan, Z. Ali, et al., Synthesis of stable benzimidazole derivatives bearing pyrazole as anticancer and EGFR receptor inhibitors, Bioorg Chem. 78 (2018) 158–169.
[3] İ. Çelik, G. Ayhan-Kılcıgil, B. Güven, Z. Kara, A.S. Gurkan-Alp, A. Karayel, A. Onay-Beşikci, Design, Synthesis and Docking Studies of Benzimidazole Derivatives as Potential EGFR Inhibitors, Eur. J. Med. Chem. 173 (2019) 240–249.
[4] A.A. Nasser, I.H. Eissa, M.R. Oun, et al., Discovery of new pyrimidine-5-carbonitrile derivatives as anticancer agents targeting EGFRWT and EGFRT790M, Org. Biomol. Chem. 18 (2020) 7608–7634.
[5] C.-W. Huang, Y.-T. Chen, H.-L. Tsai, Y.-S. Yeh, W.-C. Su, C.-J. Ma, T.-N. Tsai, J.-Y. Wang, EGFR expression in patients with stage III colorectal cancer after adjuvant chemotherapy and on cancer cell function, Oncotarget 8 (2017) 114663–114676.
[6] D. Fabbro, S. Ruetz, E. Buchdunger, et al., Protein kinases as targets for anticancer agents: From inhibitors to useful drugs, Pharmacol. Ther. 93 (2002) 79–98.
[7] M.A. Shaheen, A.A. El-Emam, N.S. El-Gohary, Design, synthesis and biological evaluation of new series of hexahydroquinoline and fused quinoline derivatives as potent inhibitors of wild-type EGFR and mutant EGFR (L858R and T790M), Bioorg. Chem. 105 (2020), 104274.
[8] Z. Xiao, C. Chu, L. Zhou, Z. Zhou, Q. Zhang, F. Yang, Z. Yang, P. Zheng, S. Xu, W. Zhu, Discovery of thiapyran-pyrimidine derivatives as potential EGFR inhibitors, Bioorg. Med. Chem. 28 (2020), 115669.
[9] T.S. Mok, Y. Wu, S. Thongprasert, C. Yang, et al., Gefitinib or carboplatin-paclitaxel, N. Engl. J. Med. 361 (2009) 947–957.
[10] F.A. Shepherd, J.R. Pereira, T. Ciuleanu, Erlotinib in previously treated non–small-cell lung cancer, N. Engl. J. Med. 353 (2005) 225–237.
[11] B. Ko, D. Paucar, B. Halmos, EGFR T790M: Revealing the secrets of a gatekeeper, Lung Cancer (Auckl). 8 (2017) 147–159.
[12] H.A. Yu, Analysis of tumor specimens at the time of acquired resistance to EGFR-TKI therapy in 155 patients with EGFR-mutant lung cancers, Clin. Cancer Res. 19 (2013) 2240–2247.
[13] T.T. Phan, B. Tran, S.T. Nguyen, T.T. Ho, H.T. Nguyen, V.T. Le, A.T. Le, EGFR plasma mutation in prediction models for resistance with EGFR TKI and survival of non-small cell lung cancer, Clin. Trans. Med. 8 (2019) 4, https://doi.org/10.1186/s40169-019-0219-8.
[14] R.T. Dungo, G.M. Keating, Afatinib: first global approval, Drugs 73 (2013) 1503–1515.
[15] D. Marquez-Medina, S. Popat, Afatinib, a second-generation EGF receptor and ErbB tyrosine kinase inhibitor for the treatment of advanced non-small-cell lung cancer, Future Oncol. 11 (2015) 2525–2540.
[16] T. Mitsudomi, Dacomitinib: another option for EGFR-mutant lung cancer ? Lancet Oncol. 15 (2014) 1408–1409.
[17] Y.L. Wu, Y. Cheng, X. Zhou, et al., Dacomitinib versus gefitinib as first-line treatment for patients with EGFR-mutation-positive non-small-cell lung cancer (ARCHER 1050): a randomised, open-label, phase 3 trial, Lancet Oncol. 18 (2017) 1454–1466.
[18] J. Li, B. An, X. Song, Q. Zhang, C. Chen, S. Wei, R. Fan, X. Li, Y. Zou, Design, synthesis and biological evaluation of novel 2,4-diaryl pyrimidine derivatives as selective $EGFR^{L858R}/^{T790M}$ inhibitors, Eur. J. Med. Chem. 212 (2021), 113019.
[19] D.A. Cross, S.E. Ashton, S. Ghiorghiu, et al., AZD9291, an irreversible EGFR TKI, overcomes T790M-mediated resistance to EGFR inhibitors in lung cancer, Cancer Discov. 4 (2014) 1046–1061.
[20] M.R.V. Finlay, M. Anderton, S. Ashton, et al., Discovery of a potent and selective EGFR inhibitor (AZD9291) of both sensitizing and T790M resistance mutations that spares the wild type form of the receptor, J. Med. Chem. 57 (2014) 8249–8267.
[21] P.A. Janne, J.C. Yang, D.W. Kim, et al., AZD9291 in EGFR inhibitor-resistance non-small-cell lung cancer, N. Engl. J. Med. 372 (2015) 1689–1699.
[22] A. Murtuza, A. Bulbul, J.P. Shen, et al., Novel Third-Generation EGFR Tyrosine Kinase Inhibitors and Strategies to Overcome Therapeutic Resistance in Lung Cancer, Cancer Res. (2019), https://doi.org/10.1158/0008-5472.CAN-18-1281.
[23] X. Gao, X. Le, D.B. Costa, The safety and efficacy of osimertinib for the treatment of $EGFR^{T790M}$ mutation positive non-small-cell lung cancer, Expert Rev. Anticancer Ther. 16 (2016) 383–390.
[24] S. Wang, S. Cang, D. Liu, Third-generation inhibitors targeting EGFR T790M mutation in advanced non-small cell cancer, J. Hematol. Oncol. 34 (2016) 9–15.
[25] G. Goss, C.M. Tsai, F.A. Shepherd, et al., Osimertinib for pretreated EGFR Thr790Met-positive advanced non-small-cell lung cancer (AURA2): a multicentre, open-label, single-arm, phase 2 study, Lancet Oncol. 17 (2016) 1643–1652.
[26] J. Zhang, P.L. Yang, N.S. Gray, Targeting cancer with small molecule kinase inhibitors, Nat. Rev. Cancer 9 (1) (2009) 28–39.
[27] A.A. Gaber, A.H. Bayoumi, A.M. El-morsy, F.F. Sherbiny, A.B.M. Mehany, I. H. Eissa, Design, synthesis and anticancer evaluation of 1H-pyrazolo[3,4-d] pyrimidine derivatives as potent EGFRWT and EGFRT790M inhibitors and apoptosis inducers, Bioorg. Chem. 80 (2018) 375–395.
[28] S. Mowafy, A. Galanis, Z.M. Doctor, R.M. Paranal, D.S. Lasheen, N.A. Farag, P. A. Jänne, K.A. Abouzid, Toward discovery of mutant EGFR inhibitors; Design, synthesis and *in vitro* biological evaluation of potent 4-arylamino-6-ureido and thioureido-quinazoline derivatives, Bioorg. Med. Chem. 24 (16) (2016) 3501–3512.
[29] Z. Zhao, H. Wu, L. Wang, Y. Liu, S. Knapp, Q. Liu, N.S. Gray, Exploration of type II binding mode: a privileged approach for kinase inhibitor focused drug discovery? ACS Chem. Biol. 9 (6) (2014) 1230–1241.
[30] P. Furet, G. Caravatti, N. Lydon, J.P. Priestle, J.M. Sowadski, U. Trinks, P. Traxler, Modelling study of protein kinase inhibitors: binding mode of staurosporine and origin of the selectivity of CGP 52411, J. Comput. Aided Mol. Des. 9 (6) (1995) 465–472.
[31] Y. Liu, N.S. Gray, Rational design of inhibitors that bind to inactive kinase conformations, Nat. Chem. Biol. 2 (7) (2006) 358–364.

[32] P. Callery, G. Peter, Cancer and cancer chemotherapy, in: A.W. David, L.L. Thomas (Eds.), Foye's principles of medical chemistry, Williams and Wilkins, Lippincott, Philadelphia, 2002.
[33] H. Shao, S. Shi, D.W. Foley, et al., Synthesis, structure–activity relationship and biological evaluation of 2, 4, 5-trisubstituted pyrimidine CDK inhibitors as potential anti-tumor agents, Eur. J. Med. Chem. 70 (2013) 447–455.
[34] K.R.A. Abdellatif, R.B. Bakr, Pyrimidine and fused pyrimidine derivatives as promising protein kinase inhibitors for cancer treatment, Med. Chem. Res. 30 (2020) 31–49.
[35] N.M. Saleh, M.G. El-Gazzar, H.M. Aly, R.A. Othman, Novel Anticancer Fused Pyrazole Derivatives as EGFR and VEGFR-2 Dual TK Inhibitors, Front. Chem. (2020), https://doi.org/10.3389/fchem.2019.00917.
[36] F. Nawaz, O. Alam, A. Perwez, et al., Design, Synthesis, Molecular Docking, and Anticancer Evaluation of Pyrazole Linked Pyrazoline Derivatives with Carbothioamide Tail as EGFR Kinase Inhibitors, Anticancer Agents Med. Chem. 21 (1) (2021) 42–60.
[37] A.R. Sayed, S.M. Gomha, F.M. Abdelrazek, M.S. Farghaly, S.A. Hassan, P. Metz, Design, efficient synthesis and molecular docking of some novel thiazolyl-pyrazole derivatives as anticancer agents, BMC Chem. 13 (2019) 116.
[38] T.T.H. Hajalsiddig, A.M. Osman, A.E.M. Saeed, 2D-QSAR Modeling and Molecular Docking Studies on 1H-Pyrazole-1-carbothioamide Derivatives as EGFR Kinase Inhibitors, ACS Omega 5 (2020) 18662–18674.
[39] B. Bhattachary, S. Mukherjee, Cancer Therapy Using Antibiotics, J. Cancer Res. Ther. 6 (2015) 849–858.
[40] O. Tacar, P. Sriamornsak, C.R. Dass, Doxorubicin: An Update on Anticancer Molecular Action, Toxicity and Novel Drug Delivery Systems, J. Pharm. Pharmacol. 65 (2013) 157–170.
[41] P. Skehan, R. Storeng, D. Scudiero, A. Monks, J. McMahon, D. Vistica, J.I. Warren, H. Bokesch, S. Kenney, M.R. Boyd, New colorimetric cytotoxicity assay for anticancer-drug screening, J. Nat. Cancer Inst. 82 (1990) 1107–1112.
[42] A.E. Amr, E.A. Elsayed, M.A. Al-Omar, H.O. Badr Eldin, E.S. Nossier, M. M. Abdallah, Design, synthesis, anticancer evaluation and molecular modeling of novel estrogen derivatives, Molecules 24 (2019) 416.
[43] L.A.H. van Bergen, M. Alonso, A. Palló, L. Nilsson, F.D. Proft, J. Messens, Revisiting sulfur H-bonds in proteins: The example of peroxiredoxin AhpE, Sci. Rep. 6 (2016) 3036.
[44] Y. Jia, C.M. Quinn, A.I. Gagnon, R. Talanian, Homogeneous time-resolved fluorescence and its applications for kinase assays in drug discovery, Anal. Biochem. 356 (2) (2006) 273–281.
[45] I.M.M. Othman, M.A.M. Gad-Elkareem, A.E. Amr, M.A. Al-Omar, E.S. Nossier, E. A. Elsayed, Novel heterocyclic hybrids of pyrazole targeting dihydrofolate reductase: design, biological evaluation and in silico studies, J. Enzyme Inhib. Med. Chem. 35 (2020) 1491–1502.
[46] A.B. Sabti, A.A. Al-Fregi, M.Y. Yousif, Synthesis and Antimicrobial Evaluation of Some New Organic Tellurium Compounds Based on Pyrazole Derivatives, Molecules 25 (2020) 3439.
[47] H. Kumar, K.K. Bansal, A. Goyal, Synthetic Methods and Antimicrobial Perspective of Pyrazole Derivatives: An Insight, AntiInfect. Agents Med. Chem. 18 (3) (2020) 207–223.
[48] H.S. Ibrahim, W.M. Eldehna, H. Abdel-Aziz, M.M. Elaasser, M.M. Abdel-Aziz, Improvement of antibacterial activity of some sulfa drugs through linkage to certain phthalazin-1(2*H*)-one scaffolds, Eur. J. Med. Chem. 85 (2014) 480–486.
[49] C. Perez, M. Pauli, P. Bazevque, An antibiotic assay by the agar well diffusion method, Acta. Biol Med Exp. 15 (1990) 113–115.
[50] A.C. Scott, J.G. Collee, J.P. Duguid, A.G. Fraser, B.P. Marmion, in: Laboratory Control of Antimicrobial Therapy Mackie and Mac-Cartney Practical Medical Microbiology, thirteenth ed., Churchill Livingstone, 1989, pp. 161–181.
[51] Y.M. Syam, M.M. Anwar, E.R. Kotb, S.A. Elseginy, H.M. Awad, G.E.A. Awad, Development of Promising Thiopyrimidine-Based Anti-cancer and Antimicrobial Agents: Synthesis and QSAR Analysis, Mini Rev. Med. Chem. 19 (2019) 1255–1276.
[52] E.S. Nossier, S.M. El-Hallouty, E.R. Zaki, Synthesis, anticancer evaluation and molecular modeling of some substituted thiazolidinonyl and thiazolyl pyrazole derivatives, Int. J. Pharm. Sci. 7 (2015) 353–359.
[53] E.S. Nossier, S.S. Abd El-Karim, N.M. Khalifa, A.S. El-Sayed, E.S.I. Hassan, S.M. El-Hallouty, Kinase inhibitory activities and molecular docking of a novel series of anticancer pyrazole derivatives, Molecules 23 (2018) 3074.
[54] X.E. Yan, P. Ayaz, S.J. Zhu, et al., Structural basis of AZD9291 selectivity for EGFR ^{T790M}, J. Med. Chem. 63 (2020) 8502–8851.
[55] I.M.M. Othman, M.A.M. Gad-Elkareem, M. El-Naggar, E.S. Nossier, A.E. Amr, Novel phthalimide based analogues: Design, synthesis, biological evaluation, and molecular docking studies, J. Enzyme Inhib. Med. Chem. 34 (2019) 1259–1270.
[56] J. Brahmi, S. Bakari, S. Nasri, A. Kadri, H. Nasri, K. Aouadi, Synthesis and SPAR exploration of new semicarbazone-triazole hybrids in search of potent antioxidant, antibacterial and antifungal agents, Mol. Biol. Rep. 46 (2019) 679–686.
[57] S.R. Prasanna Doerksen, Topological polar surface area: a useful descriptor in 2DQSAR, J. Cur Med. Chem. 16 (2009) 21–41.
[58] K.A. Khan, H.M. Faidallah, 1-Substituted carbamoyl and thiocarbamoyl-4,5-dihydro-1*H*-pyrazoles as possible cytotoxic and antimicrobial agents, J. Enzyme Inhib. Med. Chem. 31 (2016) 619–627.
[59] The OSIRIS property explorer software. Available from: http://www.organic-chemistry.org/prog/peo/.
[60] M.R.P. Queiroz, I.C.F.R. Ferreira, Y.D. Gaetano, G. Kirsch, R.C. Calhelha, L. M. Estevinho, Synthesis and antimicrobial activity studies of orthochlorodiarylamines and heteroaromatic tetracyclic systems in the benzo[b] thiophene series, Bioorg. Med. Chem. 14 (2006) 6827–6831.